Review

Not peer-reviewed version

Spin Demographics of Active Supermassive Black Holes: Updated Estimates from X-Ray Reflection and Future Opportunities

Júlia M. Sisk-Reynés *, Christopher S. Reynolds, James H. Matthews, Dominic J. Walton, Joanna M. Piotrowska, James F. Steiner, Javier A. García, Angelo Ricarte

Posted Date: 9 April 2026

doi: 10.20944/preprints202604.0638.v1

Keywords: supermassive black holes

Review

Spin Demographics of Active Supermassive Black Holes: Updated Estimates from X-Ray Reflection and Future Opportunities †

Júlia M. Sisk-Reynés [1,*], Christopher S. Reynolds [2], James H. Matthews [3], Dominic J. Walton [4], Joanna M. Piotrowska [5], James F. Steiner [1], Javier A. García [6] and Angelo Ricarte [1,7]

[1] Center for Astrophysics | Harvard & Smithsonian, Cambridge, MA 02138, USA
[2] Department of Astronomy, University of Maryland, College Park, MD 20742, USA
[3] Department of Physics, Astrophysics, University of Oxford, Denys Wilkinson Building, Keble Road, Oxford OX1 3RH, UK
[4] Centre for Astrophysics Research, Department of Physics, Astronomy and Mathematics, University of Hertfordshire, College Lane, Hatfield AL109AB, UK
[5] Cahill Center for Astronomy & Astrophysics, California Institute of Technology, Pasadena, CA 91125, USA
[6] X-Ray Astrophysics Laboratory, NASA Goddard Space Flight Center, Greenbelt, MD 20771, USA, USA
[7] Black Hole Initiative at Harvard University, 20 Garden Street, Cambridge, MA 02138, USA
* Correspondence: julia.sisk_reynes@cfa.harvard.edu
† Submitted to Galaxies on March 24, 2026 as an invited contribution to the 'X-Ray Probes of Black Hole Spin and Accretion Physics' Special Issue. Comments welcome!

Abstract

Understanding the growth of supermassive black holes (SMBHs) requires observational constraints on how their angular momentum – or spin – varies with mass, since the relative importance of coherent accretion, chaotic accretion, and mergers will be reflected in SMBH spin populations. Here we present an updated compilation of reflection-based SMBH spin measurements from the literature and assemble a set of ancillary quantities of interest for each SMBH (including redshift, Eddington ratio, and X-ray luminosity). We find no obvious correlation between the Eddington ratio and the reflection-inferred spin in the sample. We discuss the limitations of using this heterogeneous mass–spin sample to test predictions of SMBH growth from semi-analytic models and cosmological simulations, emphasizing the need for a more uniform sample. We then highlight the encouraging prospects enabled by the next-generation *NewAthena* X-ray flagship observatory. Finally, we summarize how hierarchical Bayesian population inference applied to observed SMBH mass–spin populations will constitute a powerful framework for confirming tentative mass–spin trends in future samples.

Keywords: supermassive black holes

1. Introduction

The no-hair theorem of General Relativity states that astrophysical (uncharged) black holes are described by two fundamental quantities: black hole mass, $M_{\rm BH}$ and angular momentum, $\mathbf{J}$, or spin. The spin is commonly expressed as a dimensionless parameter $a^* = c\,\mathbf{J}/G_{\rm N}\,M_{\rm BH}^2$, where c is the speed of light in the vacuum and $G_{\rm N}$ is Newton's gravitational constant. For a Kerr (spinning) black hole, a^* must be within ± 1, where negative (positive) values of a^* denote orbits that are counter-rotating (co-rotating) with respect to the black hole spin. As first demonstrated by Ref. [3], a hole spun up by prolonged prograde accretion will inevitably be spun down by the capture of counter-rotating photon orbits, imposing the canonical upper limit on the spin magnitude of a Kerr black hole of $a^* = +0.998$.

In addition to being a fundamental property, the spins of supermassive black holes (SMBHs) in active galactic nuclei (AGN) act as fossil records of SMBH growth. One key question is the coherence of the angular momentum of inflowing material as the SMBH grows. In some semi-analytic models

 doi:10.20944/preprints202604.0638.v1

(SAMs) of hierarchical structure formation, SMBHs with $\log(M_{\rm BH}/M_\odot) \lesssim 8$ primarily grow via ordered or coherent accretion via thin-disks, leading to high-spin SMBHs in galaxies like the Milky Way [11,49]. Other SAMs also show that a prolonged phase of incoherent gas accretion would spin black holes down [39]. For instance, Ref. [21] showed that late-time incoherent (chaotic) accretion will lower the average spin of SMBHs in local AGN across mass scales. Since the characteristic spin-up and spin-down timescales in SAMs are frequently sensitive to the physical (rather than Eddington) accretion rate $\dot{m}$, transitions between radiatively inefficient and efficient accretion modes can further accelerate or suppress this mass–spin evolution [77,120].

For SMBHs with magnetized accretion flows, spin can also be decreased as spin energy is transformed into jet power via the Blandford Znajek (BZ) mechanism [4,34,103,114]. By fitting General Relativistic Magnetohydrodynamics (GRMHD) simulations, Ref. [110] proposed a model in which significant spin-down occurs whenever the disk becomes geometrically thick, at either highly sub-Eddington or super-Eddington accretion rates. These formulae were then placed in a SAM demonstrating observationally testable spin moderation via this process even when accretion proceeds in a purely coherent fashion [127]. Exploring the magnitude of BZ-driven spin-down in different simulation setups is an active area of research. Using GRMHD simulations with radiative cooling, Ref. [123] proposed a universal equilibrium spin value of $a^* \approx 0.3$ for luminous strongly magnetized accretion flows. Meanwhile, using multi-zone GRMHD simulations from the event horizon to the Bondi radius, Ref. [129] find less constant jets, and therefore longer equilibrium timescales than Refs. [103,110] by a factor of a few.

Over the past decade, hydrodynamical simulations of cosmic structure formation have started incorporating sub-grid prescriptions to account for SMBH spin evolution. Recently, Ref. [118] ran a cosmological simulation with OpenGadget3 code using a novel sub-resolution prescription to track the black hole spin by accounting for the effects of coalescence and misaligned accretion through a geometrically thin, optically thick accretion disk. Ref. [118] found that low-mass holes ($M_{\rm BH} < 10^7 M_\odot$) grow primarily through gas accretion, occurring mostly in a coherent fashion that favors spin-up. At higher masses ($M_{\rm BH} > 10^7 M_\odot$), the gas angular momentum directions of subsequent accretion episodes were often found to be uncorrelated. A high level of correlation between counter-rotating accretion and black hole spin-down was thus inferred at masses $> 10^7 M_\odot$ – a regime where SMBH coalescence was also identified to be an important growth channel. Overall, Ref. [118] concluded that the spin distributions from their simulation display a wide variety of histories, depending on the dynamical state of the gas feeding the black hole and the relative contribution of mergers and gas accretion. Other state-of-the-art numerical models also highlight that the efficiency of spin evolution is strongly tied to the instantaneous accretion rate: at fixed $\dot{m}$, low-mass SMBHs can undergo rapid spin-up on short timescales, whereas massive SMBHs require substantially longer periods of sustained coherent inflow to appreciably change their spin [120].

Here we outline the prospects of utilizing observed SMBH mass–spin populations with current and future samples to test predictions of SMBH growth from SAMs and hydrodynamic simulations, where spins estimates are drawn from X-ray reflection spectroscopy. These reflection-based estimates are expected to trace the innermost flow onto holes whose surrounding accretion disks are geometrically thin and optically thick in the Shakura-Sunyaev regime [1,2]. Therefore, we do not consider spin estimates based on other methods[1]. We have made the set of archival SMBH mass and reflection-inferred spin estimates compiled here publicly available on GitHub to enable continuous updates as new constraints become available or existing ones are revisited. A full quantitative analysis of the spin–mass distribution, including forward-modeling and population-level inference, will be presented in a separate contribution within a *NewAthena* Special Issue under preparation for publication in *JHEAP*.

[1] Other spin inference methods may include VLBI imaging and polarization signatures, using empirical and fundamental-plane relations in AGN samples, using a thick disk interpretation to describe the soft X-ray spectrum of tidal disruption events; and SED fitting (see Refs. [59,85,98,107,112,125]).

 doi:10.20944/preprints202604.0638.v1

Our contribution is organized as follows. In Section 2, we present the updated SMBH mass–spin sample with reflection-inferred spins compiled from the literature, together with several ancillary quantities of interest – including redshift, Eddington ratio and X-ray luminosity ($2-10$ keV observed frame). We then interpret this observed mass–spin plane and find no obvious correlation between the Eddington-scaled accretion rate and the black hole spin. We then outline the caveats associated with using the current observed mass–spin sample to test predictions of SMBH growth models which predict that accretion-driven and accretion+merger-driven growth would imprint different expected trends in the mas–spin plane. The caveats we highlight arise from the present limitations in sample size, heterogeneity, and statistical and systematic uncertainties. Considering the heterogeneity of reflection-based spin inference in the current literature we then argue that hierarchical Bayesian inference approaches hold a promising pathway to confirming the presence of possible mass–spin trends in observed populations. Finally, we introduce *NewAthena*'s encouraging prospects in enabling such an assessment.

NewAthena is the European Space Agency's next-generation flagship-class X-ray observatory, planned for launch in 2037 with unprecedented survey and spectroscopic capabilities [131–135]. With its large collecting area ($1-1.4$ m^2 at 1 keV), broad bandpass ($0.1-12$ keV), and the exceptional spectral resolution of its X-IFU microcalorimeter (<5 eV), *NewAthena* will resolve broad and narrow reflection features in the iron K band of nearby AGN that could be degenerate with relativistically smeared reflection. *NewAthena* will also extend reflection-based spin inference into a high redshift regime ($z \lesssim 1.5$) in distant AGN whose Fe K band is redshifted into *NewAthena*'s bandpass. *NewAthena*'s strategic survey of at least 50 new nearby SMBHs is expected to deliver the pathway towards a robust observational discrimination between accretion-driven versus accretion+merger-driven growth from observed mass–spin trends in the local universe.

2. The Observed SMBH Mass vs. Spin Plane with Reflection-Inferred Spins

The spin vs. mass plane for most moderately accreting SMBHs with existing spin estimates from X-ray reflection spectroscopy – compiled from published journal articles at the time of writing – is shown in Figure 1. This suggests a tentative decrease in spin at masses $> 10^8 M_\odot$, which may be indicative of merger-driven growth. In contrast, a distinct low-mass ($10^{6-7} M_\odot$) population of SMBHs with high-to-maximal spins ($a^* \sim 0.998$) seems to emerge, suggestive of coherent-accretion-driven growth [89,120]. This potential trend is illustrated by the gray arrow in Figure 1. If not solely the result of selection effects, the absence of retrograde spins in the current sample may place meaningful constraints on the contribution of prolonged chaotic accretion – as this would yield a broader mass–spin distribution (including retrograde values). This absence is also indicative of the important role of coherent accretion in driving SMBH growth. The exclusion of maximal spin values at 90% confidence in several SMBHs indicate that these SMBH are spun down by other processes, e.g. mergers.

 doi:10.20944/preprints202604.0638.v1

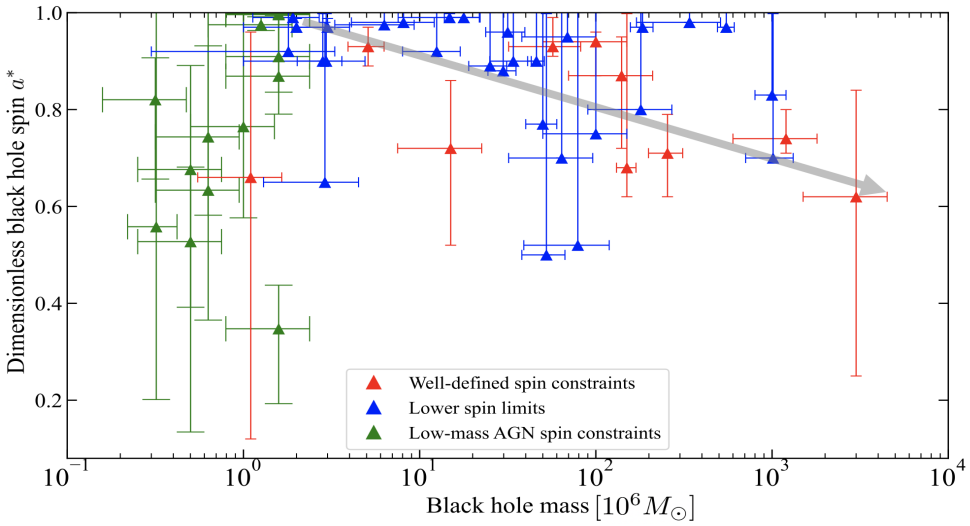

Figure 1. Observed SMBH mass–spin plane with reflection-inferred spins compiled from published literature (data listed in Table 1; error bars in spin and mass show the 90% and 68% confidence levels, respectively). The plane comprises: 10 (red) and 28 (blue) SMBHs with well-defined vs. lower spin bounds updated from the spin reviews in Refs. [88,94]; and 13 low-mass AGN (green) presented in Ref. [102]. The gray arrow marks the expectation from theory, as described in the text.

 doi:10.20944/preprints202604.0638.v1

Table 1. Spin as a function of mass for 38 SMBHs from an updated literature compilation of Ref. [94] (where the first 10 rows distinguish those with well-defined spin estimates), combined with the 13 low-mass AGN with X-ray-reflection-inferred spins from Ref. [102] (shown in the last 13 rows; see table 1 of Ref. [102] for each source's full name). Rows are ordered by decreasing mass. The error bars in mass and spin correspond to the 90% and 68% statistical uncertainties, respectively. The third column in the table references the respective papers from which we quote the mass and spin estimates for each source. The last column indicates the optical spectral classification, where we make use of the following abbreviations: Rq: radio-quiet – Ri: radio-intermediate – Q: quasar – 1 (2) : type-1 (type-2) – Sy: Seyfert – BLRG: broad-line radio galaxy – NL: narrow-line – Lensed: gravitationally lensed – BAL: broad-absorption-line.

Source	$M_{\rm BH}[10^6 M_\odot]$	Spin a^*	Refs.	Type
H 1821+643††	$(3.0^{+1.5}_{-1.5})\times10^3$	$0.62^{+0.22}_{-0.37}$	[63,105]	RqQ,1
Q 2237+305††	$(1.2^{+0.6}_{-0.6})\times10^3$	$0.76^{+0.06}_{-0.03}$	[48,91]	Lensed Q,1
Fairall 9†	255^{+56}_{-56}	$0.71^{+0.08}_{-0.09}$	[10,36]	NL,Sy,1
Ark 120†	150^{+19}_{-19}	$0.64^{+0.32}_{-0.06}$	[10,79]	Sy1
RX J1131-1231†	140 ± 70	$0.87^{+0.08}_{-0.15}$	[50,50]	Lensed Q,1
IRAS 09149–6206*	$(1.0^{+0.5}_{-0.5})\times10^2$	$0.94^{+0.02}_{-0.07}$	[64,80]	Sy1
PG 1229+204†	57^{+25}_{-25}	$0.93^{+0.06}_{-0.02}$	[10,78]	Sy1
Swift J2127.4+5654	$15.0^{+7.5}_{-7.5}$	$0.72^{+0.14}_{-0.20}$	[64,78]	Sy1
NGC 5506	$5.1^{+1.18}_{-1.18}$	$0.93^{+0.04}_{-0.04}$	[24,74]	NL,Sy1
Mrk 359′	$1.10^{+0.55}_{-0.55}$	$0.66^{+0.30}_{-0.54}$	[13,42]	NL,Sy1
PG 1426+015†	$(1.0^{+0.3}_{-0.3})\times10^3$	>0.70	[10,128]	Rq,Sy1
PG 2112+059	$(1.0^{+0.2}_{-0.2})\times10^3$	>0.83	[16,29]	BAL,Q
PG 0804+761′	550^{+60}_{-60}	>0.97	[13,78]	Rq,1
1 H0419-577	340^{+170}_{-170}	>0.98	[26,70]	Rq,Sy1
Mrk 1501††	184^{+27}_{-27}	>0.97	[35,81]	Ri,1
RBS 1124†	180^{+90}_{-90}	>0.236	[10,115]	Rq,Q
Fairall 51	$(1.0^{+0.5}_{-0.5})\times10^2$	>0.6	[14,57]	Sy1
Mrk 841	79^{+40}_{-40}	>0.52	[13,42]	Rq,Sy1
IRAS 13197-1627′	64^{+34}_{-34}	>0.7	[13,75]	Sy1.8
3C 120†	60^{+31}_{-31}	>0.95	[10,40]	BLRG
Mrk 79†	$52.4^{+14.4}_{-14.4}$	>0.5	[10,78]	Sy1.2
IRAS 0521–7054′	50^{+10}_{-10}	>0.77	[86,86]	Sy2
NGC 4151†	50^{+10}_{-10}	>0.9	[54,97]	Sy1.5
1 H0323+342†	34^{+9}_{-9}	>0.9	[65,68]	NL,Sy1
ESO 033-G002′	$31.6^{+7.9}_{-7.9}$	>0.96	[96,96]	Rq,Sy2
NGC 3783*	$25.4^{+9.0}_{-7.2}$	>0.88	[33,87]	BAL,Sy1
Mrk 110†	$25.1^{+6.1}_{-6.1}$	>0.89	[10,78]	NL,Sy1
Mrk 335†	$17.8^{+4.0}_{-4.0}$	>0.91	[10,55]	NL,Sy1
PG 1535+547	$14.8^{+7.2}_{-7.2}$	>0.99	[90,130]	NL,Sy1
ESO 362-G18	$12.5^{+4.5}_{-4.5}$	>0.92	[43,43]	Sy1.5
Tons 180′	$8.1^{+4.0}_{-4.0}$	>0.98	[13,78]	NL,Sy1
IRAS 13224-3809′	$6.3^{+3.0}_{-3.0}$	>0.975	[13,69]	NL,Sy1
1 H0707-495′	$3.0^{+1.0}_{-1.0}$	>0.97	[13,32]	NL,Sy1
MCG–06-30-15†	$2.9^{+1.6}_{-1.6}$	>0.65	[58,121]	NL,Sy1
Mrk 1044	$2.82^{+0.90}_{-0.73}$	>0.9	[53,71]	NL,Sy1
Ark 564	$2.3^{+2.6}_{-1.3}$	>0.9	[78,101]	NL,Sy1
NGC 1365	$2.0^{+1.0}_{-1.0}$	>0.97	[25,52]	Sy1.5-1.8
Mrk 766′	$1.8^{+0.5}_{-0.5}$	>0.92	[13,67]	NL,Sy1
J0107††	$10^{-1}\times(16.0^{+16.0}_{-8.0})$	$0.87^{+0.08}_{-0.24}$	[17,102]	NL,Sy1
J0940††	$10^{-1}\times(16.0^{+16.0}_{-8.0})$	$0.996^{+0.001}_{-0.015}$	[17,102]	NL,Sy1
J1357††	$10^{-1}\times(16.0^{+16.0}_{-8.0})$	$0.35^{+0.15}_{-0.09}$	[17,102]	NL,Sy1
J1541††	$10^{-1}\times(16.0^{+16.0}_{-8.0})$	$0.91^{+0.07}_{-0.21}$	[17,102]	BL,Sy1
J1559††	$10^{-1}\times(16.0^{+16.0}_{-8.0})$	>0.975	[17,102]	NL,Sy1
J1140††	$10^{-1}\times(12.6^{+12.5}_{-6.3})$	$0.975^{+0.012}_{-0.016}$	[17,102]	NL,Sy1
J1347††	$10^{-1}\times(10.0^{+10.0}_{-5.0})$	$0.77^{+0.19}_{-0.43}$	[17,102]	NL,Sy1
J1434††	$10^{-1}\times(6.3^{+6.3}_{-3.1})$	$0.63^{+0.27}_{-0.45}$	[17,102]	Sy1
J1631††	$10^{-1}\times(6.3^{+6.3}_{-3.1})$	$0.76^{+0.16}_{-0.19}$	[17,102]	BL,Sy1
J1023††	$10^{-1}\times(5.0^{+5.0}_{-2.5})$	$0.53^{+0.39}_{-0.15}$	[17,102]	NL,Sy1
J1626††	$10^{-1}\times(5.0^{+5.0}_{-2.5})$	$0.68^{+0.28}_{-0.21}$	[17,102]	Sy1.5
J0228††	$10^{-1}\times(3.2^{+3.1}_{-1.6})$	$0.82^{+0.16}_{-0.09}$	[17,102]	BL,Sy1
POX 52††	$10^{-1}\times(3.2^{+3.1}_{-1.6})$	$0.56^{+0.36}_{-0.46}$	[22,102]	Sy1.8

[1] Black hole mass estimated via: optical reverberation mapping†; $H\alpha$, $H\beta$ or CIV widths, combined with a subsequent fit of virial scaling relations††; VLTI GRAVITY interferometry*; an empirical method based on observed correlations between the equivalent width attributed to narrow-line 6.4 Fe Kα emission′; and other methods (no symbol).

 doi:10.20944/preprints202604.0638.v1

2.1. Updated Mass–Spin Plane

The mass–spin estimates shown in Table 1 are an updated version of table 1 of the spin review of Ref. [94], incorporating the following changes:

- For the high-mass SMBH H 1821+643, we adopt the spin estimate in Ref. [105] (consistent with the prior bound of Ref. [51]). We note that Ref. [12] argued that the iron K band can be described with a model featuring absorption and distant reflection.
- For the extreme galaxy ESO 033-G002, we quote the mass and spin reported in Ref. [96] – consistent with the spin later estimated by Ref. [124] under a disk reflection spectrum for an extended (ring) coronal geometry.
- For Fairall 9, we consider the spin estimate inferred from spectral modeling of multi-epoch *XMM-Newton* and *Suzaku* observations of Ref. [36] without the inclusion of a model component for the soft excess in the *Suzaku* data (as such an inclusion otherwise drives the spin constraint, as detailed in their discussion). We note that several works have argued that relativistically-broadened Fe Kα emission is not required to describe the X-ray spectrum [66] or the X-ray variability [109] of Fairall 9.
- For the Seyfert 1.5 galaxy NGC 4151, we adopt the lower spin bound $a^* > 0.9$ found from an X-ray reflection fit to a joint *Swift+Suzaku* spectrum which assumed a lamppost coronal geometry [54]. Whilst this geometry seems to be strongly disfavored by joint *IXPE*, *XMM-Newton*, and *NuSTAR* polarimetric and spectroscopic analyses [108,113], a 2023 *XRISM* observation does reveal relativistically broadened Fe Kα emission. A new spin constraint from this *XRISM* observation is anticipated [119].
- We include 13 low-mass AGN sample spin estimates in Ref. [102], who used a relativistic reflection model to describe the soft excess in *XMM-Newton* data.
- We do not include the spin constraints for both IRAS 13349+2438 and the high-mass broad-line radio galaxy 4C 74.26, for the reasons outlined in section 6 of Ref. [105].
- We do not consider the spin estimate for NGC 4051 of Ref. [37], as its spin was fixed to the canonical upper limit in their spectral analysis.
- For the canonical type-1 AGN MCG–6-30-15, we conservatively adopt the time-average spin estimate of Ref. [121] ($a^* > 0.65$) from a quasi-simultaneous *XRISM*, *XMM-Newton*, and *NuSTAR* campaign. A revisited spin bound based on time-resolved spectra from this campaign is forthcoming. We note that work prior to the launch of *XRISM* had inferred tighter spin constraints for this type-1 AGN [15,47].
- We update the mass–spin compilation of Ref. [94] with four new SMBHs: Mrk 1044 [71], ESO 033-G002 [96], PG 1426+015 [128], PG 1535+547 [130].

2.2. Interpretation of the Observed Mass–Spin Plane

The large statistical uncertainties of many existing spin estimates make a robust assessment of possible trends challenging. High-mass SMBH spin measurements – where merger-driven spin-down is expected to be most apparent – also remain scarce. Within the full sample of 51 accreting SMBHs and low-mass AGN, only 20 have well-defined upper and lower bounds, while the remaining 31 only have lower limits.

Most existing reflection-based SMBH spin measurements have been obtained on a case-by-case basis, resulting in a heterogeneous dataset with varying reflection-model assumptions and implementations. The majority of the spin estimates in Figure 1 were obtained using variants of the RELXILL relativistic X-ray reflection model [44,45,60,99], applied to either broadened Fe Kα emission and the Compton hump, or to the soft excess. Close to half of all existing spin estimates (excluding the low-mass sample from Ref. [102]) were based on broadband X-ray spectra covering both the Fe K band and the Compton hump regimes. In only approximately half of these cases (i.e. $\sim$ 25% of all 51 sources in the full sample), quasi-simultaneous *XMM-Newton+NuSTAR* observations provide the most comprehensive data: *XMM-Newton*'s spectral sensitivity is critical to probing the red wing of the

 doi:10.20944/preprints202604.0638.v1

Fe K line, while *NuSTAR*'s high-energy coverage (whose bandpass covers $3-79$ keV) constrains the Compton hump, which is essential for reducing spectral modeling degeneracies.

At present, the disk reflection spectrum of only one accreting SMBH (MCG–06-30-15) has been probed with joint *XRISM+XMM-Newton+NuSTAR* coverage [121], although similar sensitivity is expected for ongoing and future *XRISM* targets (including NGC 4151; see Ref. [119]). With the unprecedented spectral resolution of *XRISM*/Resolve (~ 5 eV), the highest-precision, near-future spin measurements prior to *NewAthena* are still forthcoming.

Beyond model-dependent systematic uncertainties (which we expand on in Section 3), spin-dependent observational biases must also be considered. For a given accretion rate $\dot{m}$ onto the black hole, high-spin SMBHs (i.e. more luminous SMBHs) are overrepresented in flux-limited samples due to the spin-dependent radiative efficiency $\eta(a^*)$ [33,117]. This effect is suggested in Figure 2, showing that, for a given estimated spin, SMBHs with higher intrinsic X-ray fluxes are more abundant compared to fainter AGN.

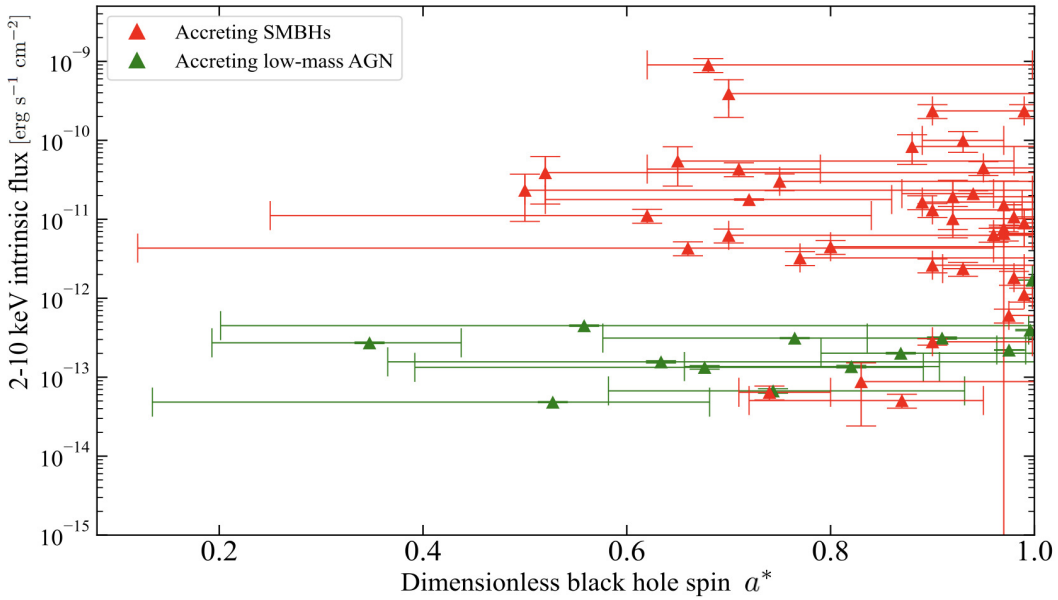

Figure 2. Intrinsic (rest-frame) X-ray flux vs. black hole spin estimated for the full sample of accreting low-mass AGN and SMBHs with reflection-inferred spins. The corresponding fluxes were estimated using the X-ray luminosity values listed in Table 2 by computing each source's luminosity distance assuming the *Planck* 2018 set of cosmological parameters [84]. We estimate the $\sim 1\sigma$ uncertainties in the flux using those in X-ray luminosity, as follows. Where available, 1σ statistical uncertainties on the X-ray luminosity from the literature are considered; otherwise, statistical uncertainties of $\pm 20\%$ are considered.

The current observed sample is also heterogeneous in X-ray luminosity, Eddington ratio, spectral type, and redshift. Where available, these quantities are listed in Table 2.

Figure 3 shows no obvious correlation between spin and Eddington ratio for the full sample. This result appears to disfavor models claiming an Eddington-ratio dependent equilibrium spin [e.g., 110]. However, SMBHs need not be at the equilibrium spin for their Eddington ratio if the Eddington ratio fluctuates on short timescales. Considering the universal equilibrium spin of $a^* \approx 0.3$ for luminous magnetized accretion flows proposed by Ref. [123], these data could be explained if most accretion does *not* proceed in such a highly magnetized fashion.

 doi:10.20944/preprints202604.0638.v1

Table 2. Ancillary data for the sample of 10 and 28 accreting SMBHs and 13 low-mass AGN with X-ray-reflection-inferred black hole spins (where sources appear in the same order as in Table 1). Where available, each column displays: L_X, the intrinsic, absorption-corrected rest-frame $2-10$ keV X-ray luminosity; the Eddington ratio $\lambda = L_X/L_{\rm Edd}$; and the redshift, z.

Source	$L_{X,2-10}$ [10^{42} erg/s]	Eddington ratio, λ	z
H 1821+643	3.39×10^3 [105]	0.39 ± 0.20 [100]	0.299
Q 2237+305	1.30×10^3 [48]	~ 0.01 [48]	1.695
Fairall 9	~ 240 [6]	~ 0.15 [36]	0.047
Ark 120†	2.42×10^3 [79]	0.24 ± 0.08 [79]	0.033
RXJ 1131-1231†	~ 100 [50]	~ 0.07 [50]	0.658
IRAS 09149-6206†	175^{+15}_{-15} [86]	~ 0.4 [86]	0.057
PG 1229+204	~ 25 [31]	0.002 [31]	0.064
Swift J2127.4+5654	9.6 ± 0.2 [41]	$\sim 0.14 \pm 0.03$ [46]	0.015
NGC 5506††	8.5 ± 2.5 [27]	~ 0.4 [27]	0.006
Mrk 359†††	~ 3 [83]	~ 0.08 [83]	0.017
PG 1426+015†	126 [31]	~ 0.04 [128]	0.087
PG 2112+059	73 ± 53 [95]	~ 0.08 [9]	0.459
PG 0804+761	208 ± 20 [20]	~ 0.4 [72]	0.100
1 H0419-577†	315 ± 70 [70]	$\sim 0.39 \pm 0.09$ [70]	0.104
Mrk 1501†	~ 140 [5]	~ 0.1 [18]	0.089
RBS 1124†	~ 600 [28]	~ 0.145 [115]	0.208
Fairall 51	14.2 ± 3.4 [57]	~ 0.025 [57]	0.014
Mrk 841	125 ± 75 [30]	0.073 [30]	0.036
IRAS 13197-1627†	~ 240 [28]	0.05 ± 0.025 [30]	0.016
3C 120	120 [8]	~ 0.77 [8]	0.033
Mrk 79	62.6 ± 37.4 [30]	0.033 ± 0.002 [30]	0.033
IRAS 00521-7054†	~ 40 [80]	≈ 1 [86]	0.069
NGC 4151††	~ 5 [54]	$\sim 0.01 - 0.1$ [97]	0.003
1 H0323+342†	~ 25 [126]	~ 0.18 [126]	0.061
ESO 033-G002†	~ 5 [96]	~ 0.02 [96]	0.018
NGC 3783	19.9 ± 8.1 [30]	0.06 ± 0.01 [33]	0.010
Mrk 110	~ 50 [93]	~ 0.1 [93]	0.035
Mrk 335	16 ± 8 [62]	$0.005 - 0.04$ [56]	0.027
PG 1535+547†	~ 4 [130]	0.315 [130]	0.038
ESO 362-G18††	< 5.1 [43]	~ 0.02 [43]	0.012
Tons 180	~ 18 [82]	> 0.55 [82]	0.062
IRAS 13224–3809 †	6.82 [69]	0.32 ± 0.05 [69]	0.066
1 H0707-495†	NA	≈ 1 [61]	0.041
MCG–06-30-15*	8.3 ± 4.3 [30]	~ 0.08 [121]	0.008
Mrk 1044†	8.6 ± 0.8 [106]	0.34 ± 0.09 [106]	0.106
Ark 564	~ 20 [7]	NA	0.025
NGC 1365	1.3 ± 1.3 [30]	0.03 ± 0.01 [30]	0.006
Mrk 766†	7.8 ± 4.8 [30]	0.04 ± 0.02 [30]	0.013
J0107	$10^{-1} \times (31.3 \pm 0.7)$ [102]	$0.28^{+0.48}_{-0.19}$ [102]	0.077
J0940	$10^{-1} \times (37.7 \pm 0.8)$ [102]	$0.36^{+0.59}_{-0.24}$ [102]	0.061
J1357	$10^{-1} \times (85.3 \pm 1.9)$ [102]	$1.0^{+1.7}_{-0.7}$ [102]	0.106
J1541	$10^{-1} \times (37.5 \pm 1.2)$ [102]	$0.35^{+0.59}_{-0.24}$ [102]	0.068
J1559	$10^{-1} \times (40.1 \pm 0.1)$ [102]	$0.38^{+0.63}_{-0.25}$ [102]	0.031
J1140	$10^{-1} \times (38.2 \pm 0.3)$ [102]	$0.45^{+0.76}_{-0.31}$ [102]	0.081
J1347	$10^{-1} \times (33.0 \pm 0.5)$ [102]	$0.47^{+0.80}_{-0.32}$ [102]	0.064
J1434	$10^{-1} \times (3.0 \pm 0.1)$ [102]	$0.04^{+0.08}_{-0.03}$ [102]	0.028
J1631	$10^{-1} \times (3.1 \pm 0.2)$ [102]	$0.05^{+0.08}_{-0.03}$ [102]	0.043
J1023	$10^{-1} \times (12.8 \pm 0.2)$ [102]	$0.29^{+0.51}_{-0.19}$ [102]	0.099
J1626	$10^{-1} \times (3.8 \pm 0.2)$ [102]	$0.08^{+0.12}_{-0.05}$ [102]	0.034
J0228	$10^{-1} \times (18.4 \pm 0.7)$ [102]	$0.75^{+1.24}_{-0.50}$ [102]	0.072
POX 52	$10^{-1} \times (4.8 \pm 0.1)$ [102]	$0.15^{+0.15}_{-0.08}$ [102]	0.021

[1] The following notation highlights accreting SMBHs whose spins (as listed in Table 1) were inferred from either broadband multi-epoch *XMM-Newton+NuSTAR* data†, simultaneous *XMM-Newton+NuSTAR+XRISM* coverage*, other broadband datasets††, e.g., *Suzaku*/XIS+*XMM-Newton*, or no multi-epoch broadband coverage (no symbol).

Future studies using large, homogeneous samples will need to account for the known correlation between the bolometric correction and Eddington fraction (particularly if the Eddington ratio is used to estimate the bolometric luminosity from the $2-10$ keV luminosity), since neglecting this correlation could bias Eddington ratio estimates [20,64]. We note that most works in the literature adopt bolometric corrections from the observed 5 100Å luminosity. Each of these approaches carries its own caveats: the AGN contribution to L_{5100} is limited by the host-galaxy subtraction method [38], although the 5 00 Å bolometric corrections are generally preferred because they exhibit smaller intrinsic scatter than X-ray bolometric corrections. In parallel, the estimate of 2–10 keV bolometric correction is itself correlated

 doi:10.20944/preprints202604.0638.v1

with the Eddington fraction, which – if unaccounted for – can lead to systematically overestimated values of $\lambda_{\rm Edd}$ [23,64]. Figure 4 also shows no obvious correlation between spin and the 2–10 keV luminosity in the sample.

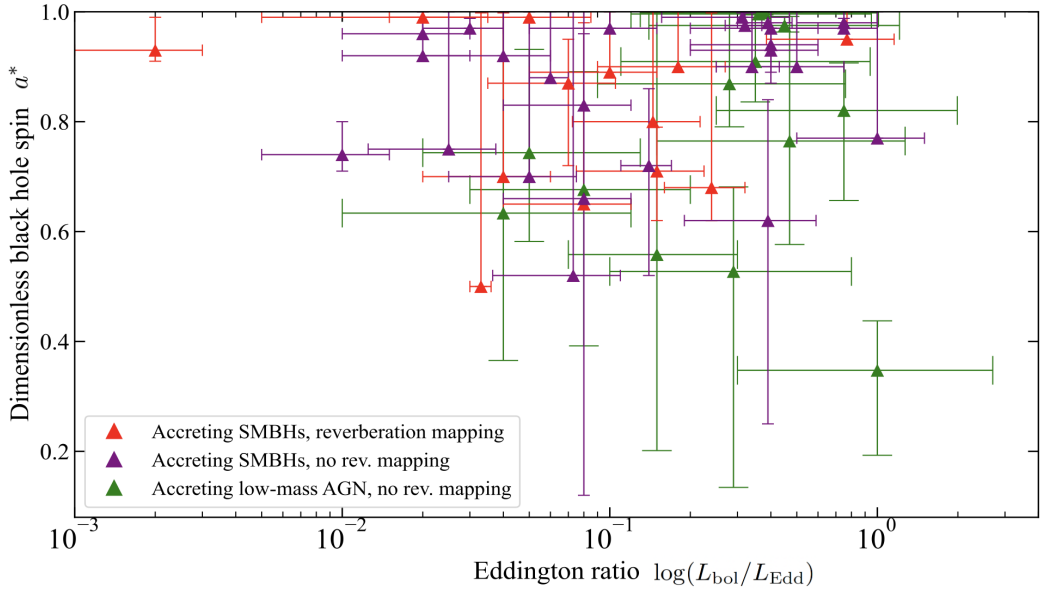

Figure 3. Black hole spin versus Eddington ratio – defined as the ratio of the bolometric luminosity to the Eddington luminosity – for the full sample of accreting low-mass AGN (green) and SMBHs (red+purple) with reflection-inferred spins. The sample of 31 accreting SMBHs is split into two distinct sub-samples: one where the black hole mass was estimated from optical reverberation mapping (red), and another where the mass was inferred by other methods (purple). The black hole masses of the 13 low-mass AGN in Ref. [102] were inferred using methods other than reverberation mapping, as specified in the text. Where available, 1σ statistical uncertainties of the Eddington ratio from the literature are considered; otherwise, statistical uncertainties of $\pm 50\%$ are shown.

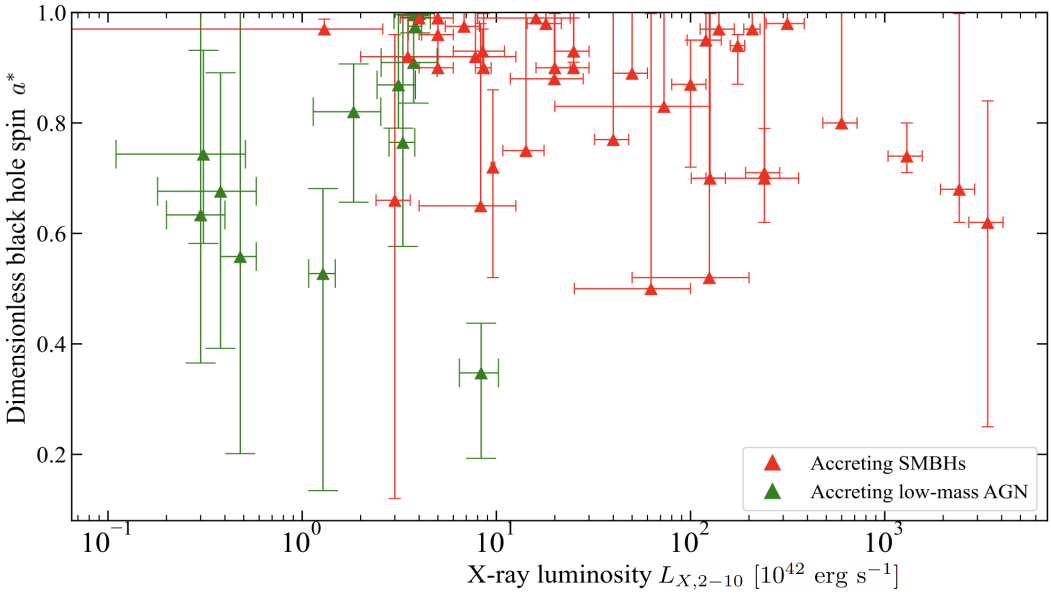

Figure 4. Black hole spin versus intrinsic (absorption-corrected) X-ray luminosity ($2-10$ keV) for the full sample of accreting low-mass AGN and SMBHs with reflection-inferred spins. Where available, 1σ statistical uncertainties on the X-ray luminosity from the literature are considered; otherwise, statistical uncertainties of $\pm 20\%$ are considered.

 doi:10.20944/preprints202604.0638.v1

3. Future Prospects: A Decisive Test of Observed Mass–Spin Trends with *NewAthena*

The current observed SMBH mass–spin sample, while invaluable, remains dominated by lower spin limits and is too heterogeneous to enable decisive tests of SMBH growth scenarios. This limitation has been demonstrated explicitly by Ref. [117], who showed that the current collection of reflection-based spin measurements at the time lacked the statistical power and uniformity required to distinguish between the distinct mass–spin trends predicted for coherent-accretion-dominated versus coherent-accretion+merger-dominated SMBH growth from the HORIZON-AGN cosmological simulation. Ref. [117] further showed that strategically sampling the SMBH mass–spin plane with the proposed *High-Energy X-ray Probe* (*HEX-P*) [116] – a mission concept with *NuSTAR*-like high-energy coverage but a substantially larger collecting area – with three mass bins would enable population-level spin measurements. Their approach drew a direct connection to the distinct accretion versus accretion+merger driven growth channels in HORIZONAGN by enabling observational tests of their distinct trends in the mass–spin plane, subject to specific requirements in sample size, mass range, and redshift coverage (outlined in section 7 of Ref. [117]).

In addition to sample size limitations, the assessment of systematic uncertainties in spin measurements is equally crucial [76]. These systematics fall broadly into two categories: (i) modeling systematics, arising from both spectral degeneracies and assumptions made by relativistic reflection models, and (ii) instrumental systematics, arising from calibration uncertainties. Recent work has also shown that within the first category, spectral model degeneracies – particularly those involving warm absorbers, ultra-fast outflows, and complex soft X-ray structure – can mimic or obscure relativistically smeared reflection features. Ref. [104] demonstrated this explicitly in the context of *NewAthena* and also showed that these degeneracies are dramatically reduced when broadband coverage is included to fully probe the Compton hump and characterize the high-energy cutoff. In parallel, a comprehensive analysis that jointly incorporates the impact of different modeling assumptions on the reflection-based spin – such as alternative coronal geometries beyond the lamppost, the use of razor-thin versus razor-thick disk prescriptions, or considering reflected emission within the innermost stable circular orbit – has yet to be completed, although several recent studies have begun to quantify how such choices can affect the recovered spin for a given underlying spin (e.g. Refs. [73,122,124]).

Within this first category, the role of disk density is also increasingly recognized as a key modeling uncertainty. Standard implementations of `relxill` assume a fixed mid-plane density of $n_e = 10^{15}\,\mathrm{cm}^{-3}$, which directly sets the ionization parameter and is known to be an oversimplification. High-density reflection models relax this assumption by allowing the density to vary, and in several cases alleviate the need for the super-solar iron abundances often inferred with fixed-density models. However, the interplay between density, ionization, and the inner disk metallicity remains poorly understood, and a systematic assessment of how high-density models impact recovered spin values has not yet been performed. In parallel, a further source of uncertainty arises from the poorly constrained inclination distribution of current reflection-based spin measurements: most studies report only approximate inclination values, preventing a proper assessment of correlations between inclination, spin, and other spectral parameters. Very high inferred inclinations can partially mimic the blueshifted wing of the broadened Fe Kα line, introducing a degeneracy that cannot yet be quantified robustly in the absence of full posterior information for most published analyses.

Within the second category, instrumental calibration remains an important consideration. Ref. [111] demonstrated that machine-learning approaches such as convolutional neural networks (when trained to distinguish astrophysical spectral features from detector-calibration artifacts in synthetic *NewAthena* spectra) offer a promising pathway towards mitigating these systematics. These developments highlight that progress in SMBH spin studies requires not only larger samples but also improved tools for disentangling physical and instrumental effects. We highlight that careful consideration of systematic uncertainties will be especially critical for *NewAthena*, whose dramatically reduced Poisson uncertain-

 doi:10.20944/preprints202604.0638.v1

ties – enabled by its much larger collecting area – will shift the limiting factor in reflection-based spin estimates from statistical noise to these systematic effects.

The upcoming *NewAthena* X-ray observatory is poised to deliver the uniform dataset of reflection-based spin estimates identified as necessary by Ref. [117], while with a mission profile distinct from *HEX-P*. *NewAthena* is currently planning a survey of at least 50 nearby SMBHs – beyond the current sample in Figure 1 – that will deliver the first homogeneous, high-precision spin catalog for the local, intermediate-mass AGN population, providing a well-characterized anchor sample for confirming tentative mass–spin predictions. As highlighted by section 7 of Ref. [117], a sample of 50 accreting SMBH may neither overcome the high-spin bias reflected in the current sample, nor uniformly populate the high-mass SMBH end ($M_{\rm BH} > 10^9 M_\odot$) in the local universe, where theoretical models of accretion-driven vs. accretion+merger-driven growth differ more significantly. Noting that at $z \sim 0$ only a handful of such massive, X-ray luminous SMBHs exist, the forthcoming *NewAthena* spin survey of at least 50 nearby AGN will be dominated by SMBHs with intermediate masses. For this reason, the current heterogeneous sample of 51 reflection-based spin estimates will remain essential for spanning the full $10^6 - 10^{10} M_\odot$ mass range required to statistically discriminate between competing mass–spin trends in cosmological models and SAMs. However, we note that many of the existing estimates will need to be revisited – and reobserved with *NewAthena* if *XRISM* follow-up is not available at the time of *NewAthena*'s launch – before such estimates can be used along with *NewAthena*'s new survey. This is particularly pressing for current spin estimates driven by the reflection interpretation of the soft excess, which has led to high a^* estimates in several Narrow-Line Seyfert 1s in the current sample. In such cases, the soft excess itself can act as the dominant driver of the spin constraint: in the absence of a pronounced broadened Fe Kα line and Compton hump, the forest of relativistically blurred soft X-ray features predicted by reflection models forces the fit toward high spin, effectively yielding lower limits that may *not* reflect the true underlying spin.

Probing spin evolution across cosmic time will require extending beyond the local sample, since a nearby survey alone cannot map redshift-dependent trends. The value of the *NewAthena* survey will instead lie in providing a well-characterized anchor sample with unprecedented sensitivity due to its improved collecting area and unprecedented spectral resolution compared to current X-ray missions. We highlight that for distant SMBHs up to $z \sim 1.5$, the rest-frame Fe K band is redshifted into *NewAthena*'s $0.1 - 12$ keV sensitivity window, enabling spin measurements for bright sources at moderate redshift without relying on strong gravitational lensing. This redshift effect opens a complementary pathway for extending spin studies beyond the local universe, although the achievable precision will depend on source brightness and exposure time.

3.1. A Statistical Framework to Probe SMBH Mass–Spin Trends with NewAthena

Hierarchical Bayesian inference offers a particularly powerful and timely tool to extract the underlying spin distribution from both current and future observed mass–spin datasets. This framework has already proven transformative in gravitational-wave astronomy, where it is routinely used by the *LVK* Collaboration to infer the underlying spin distributions of merging stellar-mass black holes from gravitational-wave signals [92]. Applying analogous techniques to *NewAthena*'s spin catalog will allow the X-ray community to start addressing if the local SMBH population reflects a mixture of coherent and incoherent accretion, SMBH mergers, and jet-induced spin-down, to quantify the relative importance of these channels at low redshift. These techniques will enable incorporating systematic uncertainties due to spectral model degeneracies, modeling assumptions, and detector calibration, to account for spin-dependent radiative-efficiency selection effects in flux-limited samples, and to enable principled comparisons between physical models of SMBH growth. Such hierarchical population analyses have not yet been attempted for SMBH spins inferred from X-ray reflection, and the first exploratory tests in the context of *NewAthena* are underway. Preliminary exploration using a small set of hyperparameters – capturing a merger-driven population as a Gaussian about a mean with moderate a^* and a truncated power-law function underlying a SMBH population growing primarily via coherent accretion – indicate that this two-component description fails to reproduce the observed

 doi:10.20944/preprints202604.0638.v1

mass–spin distribution, illustrating the need for more complex and physically motivated models. The current heterogeneous mass–spin sample of 51 SMBHs – though not yet statistically decisive – provides an ideal laboratory for developing such techniques prior to their application across the *NewAthena* dataset.

In addition to the spin constraints provided by *NewAthena*, achieving this goal will require SMBH mass estimates of the highest possible precision, drawing on complementary facilities such as the *Nancy Grace Roman Space Telescope* to provide robust black hole mass estimates. Moreover, the observational requirements implemented by Ref. [117] for the *HEX-P* spin survey will need to be revisited in the context of *NewAthena*, since its spectral capabilities, survey strategy, and redshift reach differ from those assumed in the *HEX-P* forecasts of Ref. [117]. In particular, unlike *HEX-P*, *NewAthena* will *not* have the high-energy coverage needed to fully characterize the Compton hump or robustly constrain the high-energy cutoff – essential for tight reflection-based spin estimates and to break spectral model degeneracies. Thus, assessing the impact of this limitation and determining how it could affect the distinction between competing mass–spin trends will be a central component of *NewAthena*'s SMBH spin survey.

Together, *NewAthena* and hierarchical Bayesian population modeling promise to transform SMBH spin studies in observed SMBH mass–spin distributions. Whilst this combination cannot realistically capture the full SMBH evolution in mass and redshift, it will provide the most robust and controlled benchmark of observed mass–spin trends in the local universe, transforming these observed correlations into a quantitative test of competing growth scenarios.

Data Availability Statement: All the data presented are public and available at https://github.com/joanna-pk/xray-reflection-spin-repository.

Acknowledgments: JSR acknowledges support from a NASA ADAP Program Grant 80NSSC24K0617. DJW acknowledges support from the Science and Technology Facilities Countil (STFC; grant code ST/Y001060/1). JSR thanks Labani Mallick for sharing a digitized version of the data presented in Ref. [102] and Daniel Schwartz and Laura Brenneman for comments on this manuscript.

Conflicts of Interest: The authors declare no conflicts of interest.

References

1. Shakura, N. I. & Sunyaev, R. A. *Black holes in binary systems. Observational appearance*. *A&A* **1973**, *24*.
2. Novikov, I. D. & Thorne, K. S. *Astrophysics of black holes. Black holes (Les astres occlus)* **1973**, pp. 343-450. Thorne, K. S. *Disk-Accretion onto a Black Hole. II. Evolution of the Hole*. *ApJ* **1974**, *191*.
3. Thorne, K. S. *Disk-Accretion onto a Black Hole. II. Evolution of the Hole*. *ApJ* **1974**, *191*.
4. Blandford, R. D. & Znajek, R. L. **1977**, *MNRAS*, *179*, 433
5. Schnopper, H. W., et al. *X-ray and radio emission from the compact galaxy III Zw 2*. *ApJ* **1974**, *222*, L91-L94.
6. Leighly, K. M., et al. *Long-term X-ray Variability from the Luminous AGNs Fairall 9 and 3C390.3*. **2000**, *RXTE conference*.
7. Turner, M. J. L., et al. *The European Photon Imaging Camera on XMM-Newton: The MOS cameras*. **2001**, *A&A*, **365**, p.L27-L35.
8. Ballantyne, D. R., Fabian, A. C., & Iwasawa, K. *The XMM-Newton view of the broad-line radio galaxy 3C 120*. *MNRAS* **2004**, *354*, 3.
9. Gallagher S. C., et al. *Dramatic X-Ray Spectral Variability of the Broad Absorption Line Quasar PG 2112+059*. *ApJ* **2004**, *603*, 2.
10. Peterson B. M., et al. *Central Masses and Broad-Line Region Sizes of Active Galactic Nuclei. II. A Homogeneous Analysis of a Large Reverberation-Mapping Database*. *ApJ* **2012**, *613*, p.682.
11. Volonteri, M., et al. *The Distribution and Cosmic Evolution of Massive Black Hole Spins*. *ApJ* **2005**, *620*, 1.
12. Yaqoob, T. & Serlemitsos, P. *Iron K Features in the Quasar E1821+643: Evidence for Gravitationally Redshifted Absorption?*. *ApJ* **2005**, *623*, 1.
13. Zhou, X-L. & Wang, J-M. *Narrow Iron Kα Lines in Active Galactic Nuclei: Evolving Populations*. *ApJ* **2005**, *618*, L83.

 doi:10.20944/preprints202604.0638.v1

14. Bennert, N., et al. *Size and properties of the narrow-line region in Seyfert-2 galaxies from spatially-resolved optical spectroscopy*. *A&A* **2006**, *456*, 3.
15. Brenneman, L. W. & Reynolds, C. S. *Constraining Black Hole Spin via X-Ray Spectroscopy*. *ApJ* **2006**, *652*, 2.
16. Vestegaard, M. & Peterson, B. M. *Determining Central Black Hole Masses in Distant Active Galaxies and Quasars. II. Improved Optical and UV Scaling Relationships*. *ApJ* **2006**, *641*, 689.
17. Greene, J. E & Ho, L. *A New Sample of Low-Mass Black Holes in Active Galaxies*. *ApJ* **2007**, *670*, 2.
18. Inoue, H., Terashima, Y., & Ho. L. C. *Fe K Line Profile in Low-Redshift Quasars: Average Shape and Eddington Ratio Dependence*. *ApJ* **2007**, *662*, 2.
19. Miller, L., et al. *The variable X-ray spectrum of Markarian 766*. *A&A* **2007**, *463*, 131-143.
20. Vasudevan, R. V & Fabian, A. C. *Piecing together the X-ray background: bolometric corrections for active galactic nuclei*. *MNRAS* **2007**, *381*, 3.
21. King, A., Pringle, J. E., & Hofmann, J. A. *The evolution of black hole mass and spin in active galactic nuclei*. *MNRAS* **2008**, *385*, 3.
22. Thornton, C. E., et al. *The Host Galaxy and Central Engine of the Dwarf Active Galactic Nucleus POX 52*. *ApJ* **2008**, *686*, 2.
23. Vasudevan, R. V. & Fabian, A. C. *Simultaneous X-ray/optical/UV snapshots of active galactic nuclei from XMM-Newton: spectral energy distributions for the reverberation mapped sample*. *MNRAS* **2009**, *392*, 2.
24. Nikolajuk, M., Czerny B., & Gurinowicz P. *NLS1 galaxies and estimation of their central black hole masses from the X-ray excess variance method*. *MNRAS* **2009**, *394*, 4.
25. Risaliti, G., et al. *The XMM-Newton long look of NGC 1365: uncovering of the obscured X-ray source*. *MNRAS:Letters* **2009**, *393*, 1.
26. Grupe, D., et al. *The simultaneous optical-to-X-ray spectral energy distribution of soft X-ray selected active galactic nuclei observed by Swift*. *ApJ Supplement Series* **2010**, *187*, 64-106.
27. Guainazzi, M., et al. *Final verdict from XMM-Newton: the X-ray obscured Seyfert galaxy NGC 5506 has a broad Fe Kα line*. *MNRAS* **2010**, *406*, 3.
28. Minniuti, G., et al. *Does the X-ray emission of the luminous quasar RBS 1124 originate in a mildly relativistic outflowing corona? MNRAS* **2010**, *401*, 2.
29. Schartel, N., et al. *A long hard look at the minimum state of PG 2112+059 with XMM-Newton*. *A&A* **2010**, *512*, id. A75.
30. Vasudevan, R. V., et al. *The power output of local obscured and unobscured AGN: crossing the absorption barrier with Swift/BAT and IRAS*. *MNRAS* **2010**, *402*, 2.
31. Zhou, X-L. & Zhao, Y-H. *Hard X-ray Photon Index as an Indicator of Bolometric Correction in Active Galactic Nuclei*. *ApJL* **2010**, *720*, 2.
32. Zoghbi, A., et al. *Broad iron L-line and X-ray reverberation in 1H0707-495*. *MNRAS* **2010**, *401*, 4.
33. Brenneman, L., et al. *The Spin of the Supermassive Black Hole in NGC 3783*. *ApJ* **2011**, *736*, 2, id. 103.
34. Tchekhovskoy, A., Narayan, R., & McKinney, J. C. *MNRAS*, **2011**, *418*, 1, L79.
35. Grier, C. J., et al. *Reverberation Mapping Results for Five Seyfert 1 Galaxies*. *ApJ* **2012**, *755*, 1, id60.
36. Lohfink A M., et al. *The Black Hole Spin and Soft X-Ray Excess of the Luminous Seyfert Galaxy Fairall 9*. *ApJ* **2012**, *758*, 1, id67.
37. Patrick A. R., et al. *A Suzaku survey of Fe K lines in Seyfert 1 active galactic nuclei*. *MNRAS* **2012**, *426*, 3.
38. Runnoe, J. C, Brothertorn, M. C. & Shang, Z. *Updating quasar bolometric luminosity corrections*. *MNRAS* **2012**, *422*, 1, id67.
39. Dotti, M., et al. *On the Orientation and Magnitude of the Black Hole Spin in Galactic Nuclei*. *ApJ* **2013**, *762*, 2.
40. Lohfink A. M., et al. *An X-Ray View of the Jet Cycle in the Radio-loud AGN 3C120*. *ApJ* **2013**, *772*, 2.
41. Sanfrutos, M., e al. *The size of the X-ray emitting region in SWIFT J2127.4+5654 via a broad line region cloud X-ray eclipse*. *MNRAS* **2013**, *436*, 2.
42. Walton D. J., et al. *Suzaku observations of 'bare' active galactic nuclei*. *MNRAS* **2013**, *428*, 4.
43. Agís-González, B., et al. *Black hole spin and size of the X-ray emitting region(s) in the Seyfert 1.5 galaxy ESO 362–G18*. *MNRAS* **2014**, *444*, 4.
44. Dauser, T., et al. *The role of the reflection fraction in constraining black hole spin.*. *MNRAS* **2014**, *744*, pp. L.100-L104.
45. García, J., et al. *Improved Reflection Models of Black Hole Accretion Disks: Treating the Angular Distribution of X-Rays*. *ApJ* **2014**, *782*, 2.
46. Marinucci, A., et al. *Simultaneous NuSTAR and XMM-Newton 0.5-80 keV spectroscopy of the narrow-line Seyfert 1 galaxy SWIFT J2127.4+5654*. *MNRAS* **2014**, *440*, 3.

 doi:10.20944/preprints202604.0638.v1

47. Marinucci, A., et al. *The Broadband Spectral Variability of MCG-6-30-15 Observed by NuSTAR and XMM-Newton*. *ApJ* **2014**, *787*, 1, id. 83.
48. Reynolds M T., et al. *A Rapidly Spinning Black Hole Powers the Einstein Cross*. *ApJL* **2014**, *792*, 1, id L19.
49. Sesana, A., et al. *Linking the Spin Evolution of Massive Black Holes to Galaxy Kinematics*. *ApJ* **2014**, *794*, 2.
50. Reis, R., et al. *Reflection from the strong gravity regime in a lensed quasar at redshift z = 0.658*. *Nature* **2014**, *507*, I7491.
51. Reynolds, C. S., et al. *The X-Ray Spectrum of the Cooling-flow Quasar H1821+643: A Massive Black Hole Feeding Off the Intracluster Medium*. *ApJL* **2014**, *792*, 2.
52. Walton, D. J., et al. *NuSTAR and XMM-Newton Observations of NGC 1365: Extreme Absorption Variability and a Constant Inner Accretion Disk*. *ApJ* **2014**, *788*, 1, id. 76.
53. Du, P., et al. *Supermassive Black Holes with High Accretion Rates in Active Galactic Nuclei. IV. Hβ time lags and implications for supe-Eddington accretion*. *ApJ* **2015**, *806*, 22.
54. Keck, M. L., et al. *NuSTAR and Suzaku X-ray spectroscopy of NGC 4151: Evidence for reflection from the inner accretion disk*. *ApJ* **2015**, *806*, 149.
55. Gallo, L., et al. *Suzaku observations of Mrk 335: confronting partial covering and relativistic reflection*. *MNRAS* **2015**, *446*, 1.
56. Sarma, R., et al. *Relationship between X-ray spectral index and X-ray Eddington ratio for Mrk 335 and Ark 564*. *MNRAS* **2015**, *448*, pp. 1541–1550.
57. Svoboda, J., et al. *An X-ray variable absorber within the broad line region in Fairall 51*. *A&A* **2015**, *578*, A96.
58. Bentz, M., et al. *A Reverberation-based Black Hole Mass for MCG–06-30-15*. *ApJ* **2016**, *830*, 2, id136.
59. Daly, R. A. *Spin properties of supermassive black holes with powerful outflows*. *MNRAS: Letters* **2016**, *458*, 1.
60. Dauser, T., et al. *Normalizing a relativistic model of X-ray reflection. Definition of the reflection fraction and its implementation in relxill*. *A&A* **2016**, *590*, id. A76.
61. Done, C. & Chichuan, J. *The mass and spin of the extreme Narrow Line Seyfert 1 Galaxy 1H 0707-495 and its implications for the trigger for relativistic jets*. *MNRAS* **2016**, *460*, 2.
62. Leek, L. & Ballentyne, D. R. *Revealing the accretion disc corona in Mrk 335 with multi-epoch X-ray spectroscopy*. *MNRAS* **2016**, *456*, pp. 2722–2736.
63. Shapovalova, A. I., et al *First long-term optical spectral monitoring of a binary black hole candidate E1821+643. Variability of spectral lines and continuum*. *ApJS* **2016**, *222*, 25.
64. Vasudevan, R. V., et al. *A selection effect boosting the contribution from rapidly spinning black holes to the cosmic X-ray background*. *MNRAS* **2016**, *458*, 2.
65. Wang, F., et al. *Reverberation mapping og the gamma-ray loud Narrow-Line Seyfert 1 galaxy 1H 0323+342*. *ApJ* **2016**, *824*, 149.
66. Yaqoob, T., et al. *No signatures of black hole spin in the X-ray spectrum of the Seyfert 1 galaxy Fairall 9*. *MNRAS* **2016**, *462*, 4.
67. Buisson, D. J., et al. *NuSTAR observations of Mrk 766: distinguishing reflection from absorption*. *MNRAS* **2018**, *480*, 3.
68. Ghosh, R., et al. *Broad-band spectral study of the jet-disc emission in the radio-loud narrow-line Seyfert 1 galaxy 1H 0323+342*. *MNRAS* **2018**, *479*, 2.
69. Jiang, J., et al. *The 1.5 Ms observing campaign on IRAS 13224-3809 – I. X-ray spectral analysis*. *MNRAS* **2018**, *477*, 3.
70. Jiang, J., et al. *A relativistic disc reflection model for 1H0419-577: Multi-epoch spectral analysis with XMM-Newton and NuSTAR*. *MNRAS* **2018**, *483*, 3.
71. Mallick, L., et al. *A high-density relativistic reflection origin for the soft and hard X-ray excess emission from Mrk 1044*. *MNRAS* **2018**, *479*, 1.
72. Oliver-Petrucci, P., et al. *Testing warm Comptonization models for the origin of the soft X-ray excess in AGNs*. *A&A* **2018**, *611*, id. A59.
73. Taylor, C. & Reynolds, C. S. *Exploring the Effects of Disk Thickness on the Black Hole Reflection Spectrum*. *ApJ* **2018**, *855*, 2.
74. Sun, S., et al. *Multi-epoch analysis of the X-ray spectrum of the active galactic nucleus in NGC 5506*. *MNRAS* **2018**, *478*, 2.
75. Walton, D J., et al. *Disentangling the complex broad-band X-ray spectrum of IRAS 13197-1627 with NuSTAR, XMM-Newton and Suzaku*. *MNRAS* **2018**, *473*, 4.
76. Barret, D., & Cappi, M. *Inferring black hole spins and probing accretion/ejection flows in AGNs with the Athena X-ray Integral Field Unit*. *A&A* **2019**, *628*, id. A5.

 doi:10.20944/preprints202604.0638.v1

77. Bustamante, S. & Springel, V. *Spin evolution and feedback of supermassive black holes in cosmological simulations*. *MNRAS* **2019**, *490*, 3.
78. Jiang, J., et al. *High Density Reflection Spectroscopy – II. The density of the inner black hole accretion disc in AGN Free*. *MNRAS* **2019**, *489*, 3.
79. Porquet, D., et al. *A deep X-ray view of the bare AGN Ark 120*. *A&A* **2019**, *623*, A11.
80. Walton, D. J., et al. *A low-flux state in IRAS 00521-7054 seen with NuSTAR and XMM-Newton: relativistic reflection and an ultrafast outflow*. *MNRAS* **2019**, *484*, 2.
81. Chamani, W., Karri, K., & Savolainen, T. *Joint XMM-Newton and NuSTAR observations of the reflection spectrum of III Zw 2*. *A&A* **2020**, *635*, id. A172.
82. Matzeu, G., et al. *The first broad-band X-ray view of the narrow-line Seyfert 1 Ton S180.MNRAS* **2020**, *497*, pp. 2352–2370.
83. Middei, R., et al. *The soft excess of the NLS1 galaxy Mrk 359 studied with an XMM-Newton-NuSTAR monitoring campaign*. *A&A* **2020**, *640*, A99.
84. *Planck* Collaboration. *Planck 2018 results. VI. Cosmological parameters*. *A&A* **2020**, *641*, A6.
85. Unal, C. & Loeb, A. *On Spin dependence of the Fundamental Plane of black hole activity*. *MNRAS* **2020**, *495*, 1.
86. Walton, D. J., et al. *A full characterization of the supermassive black hole in IRAS 09149-6206*. *MNRAS* **2019**, *499*, 1.
87. Amorim, A., et al. *A geometric distance to the supermassive black Hole of NGC 3783*. *A&A* **2021**, *654*, A85.
88. Bambi, C. *Towards Precision Measurements of Accreting Black Holes Using X-Ray Reflection Spectroscopy*. *Space Science Reviews* **2021**, *217*, 5, id. 65.
89. Dubois, Y., et al. *Introducing the NEWHORIZON simulation: Galaxy properties with resolved internal dynamics across cosmic time*. *A&A* **2021**, *651*, id. A109.
90. Hu, C., et al. *Supermassive Black Holes with High Accretion Rates in Active Galactic Nuclei. XII. Reverberation Mapping Results for 15 PG Quasars from a Long-duration High-cadence Campaign*. *ApJS* **2021**, *253*, 20.
91. Hutsemékers, D. & Sluse, D. *Geometry and kinematics of the broad emission line region in the lensed quasar Q2237+0305*. *A&A* **2021**, *654*, A155.
92. LVK Collaboration. *Population Properties of Compact Objects from the Second LIGO-Virgo Gravitational-Wave Transient Catalog*. *ApJ* **2021**, 913, 1.
93. Porquet, D., et al. *The first simultaneous X-ray broadband view of Mrk 110 with XMM-Newton and NuSTAR*. *A&A* **2021**, *654*, A89.
94. Reynolds, C. S. *Observational Constraints on Black Hole Spin*. *ARA&A* **2021**, *59*.
95. Saez, C., et al. *The X-rays wind connection in PG 2112+059*. *MNRAS* **2021**, *506*, 1.
96. Walton, D. J., et al. *Extreme relativistic reflection in the active galaxy ESO 033-G002*. *MNRAS* **2021**, *506*, 2.
97. Bentz, M. C., Williams, P. R., & Treu, T. *The Broad Line Region and Black Hole Mass of NGC 4151*. *ApJ* **2022**, *934*, 2, id. 168.
98. Daly, R. A. *Robust supermassive black hole spin mass-energy characteristics: a new method and results*. *MNRAS* **2022**, *517*, 4.
99. Daly, T. *The effect of returning radiation on relativistic reflection*. *MNRAS* **2022**, *514*, 3.
100. Fukuchi, H., et al. *H1821+643: The Most X-Ray and Infrared Luminous Active Galactic Nucleus (AGN) in the Swift/BAT Survey in the Process of Rapid Stellar and Supermassive Black Hole Mass Assembly*. *ApJ* **2022**, *940*, 1, id. 7.
101. Lewin, C., et al. *X-Ray Reverberation Mapping of Ark 564 Using Gaussian Process Regression*. *ApJ* **2022**, *939*, id. 119.
102. Mallick, L. *High-density disc reflection spectroscopy of low-mass active galactic nuclei*. *MNRAS* **2022**, *513*, 3.
103. Narayan, R., Chael, A., Chatterjee, K., et al. *MNRAS*, **2022**, *511*, 3, 3795.
104. Parker, M. L., et al. *The X-ray disc/wind degeneracy in AGN*. *MNRAS* **2022**, *513*, 1.
105. Sisk-Reynés J., et al. *Evidence for a moderate spin from X-ray reflection of the high-mass supermassive black hole in the cluster-hosted quasar H1821+643*. *MNRAS* **2022**, *514*, 2.
106. Barua, B. *A Search for X-Ray/UV Correlation in the Reflection-dominated Seyfert 1 Galaxy Markarian 1044*. *APJ* **2023**, 958, 1.
107. Cao, Z., et al. *The rapidly spinning intermediate-mass black hole 3XMM J150052.0+015452*. *MNRAS* **2023**, 519, 2.
108. Gianolli, V., et al. *Uncovering the geometry of the hot X-ray corona in the Seyfert galaxy NGC 4151 with IXPE*. *MNRAS* **2023**, *523*, 3.
109. Hagen, S. & Done, C. *Modelling continuum reverberation in active galactic nuclei: a spectral-timing analysis of the ultraviolet variability through X-ray reverberation in Fairall 9*. *MNRAS* **2023**, *521*, 1.

 doi:10.20944/preprints202604.0638.v1

110. Ricarte, A., Narayan, R., & Curd, B. *Recipes for Jet Feedback and Spin Evolution of Black Holes with Strongly Magnetized Super-Eddington Accretion Disks*. *ApJL* **2023**, *954*, 1, id. L22.
111. Sisk-Reynés, J. M., et al. *Physics Beyond the Standard Model with Future X-Ray Observatories: Projected Constraints on Very-light Axion-like Particles with Athena and AXIS*. *ApJ* **2023**, *951*, 1.
112. Temple, M. J. *Testing AGN outflow and accretion models with C IV and He II emission line demographics in $z \approx 2$ quasars*. *MNRAS* **2023**, 523, 1.
113. Gianolli, V., et al. *A second view on the X-ray polarization of NGC 4151 with IXPE*. *A&A* **2024**, *691*, id. A29.
114. Lowell, B., Jacquemin-Ide, J., Tchekhovskoy, A., et al. *ApJ*, **2024**, *960*, 1, 82.
115. Madathil-Pottayil, A., et al. *Exploring the high-density reflection model for the soft excess in RBS 1124*. *MNRAS* **2024**, *534*, 1.
116. Madsen, K. K., et al. *The high energy X-ray probe (HEX-P): instrument and mission profile*. *Frontiers in Astronomy and Space Sciences* **2024**, *11*, 1357834.
117. Piotrowska, J., et al. *The high energy X-ray probe (HEX-P): constraining supermassive black hole growth with population spin measurements*. *Frontiers in Astronomy and Space Sciences* **2024**, *11*, id. 1324796.
118. Sala, L., et al. *Supermassive black hole spin evolution in cosmological simulations with OPENGADGET3*. *A&A* **2024**, *685*, id. A92.
119. *XRISM* Collaboration. XRISM *Spectroscopy of the Fe Kα Emission Line in the Seyfert Active Galactic Nucleus NGC 4151 Reveals the Disk, Broad-line Region, and Torus*. *ApJL* **2024**, *1*, id. L25.
120. Beckmann, R., et al. *Black hole spin evolution across cosmic time from the NEWHORIZON simulation*. *MNRAS* **2025**, *536*, 2.
121. Brenneman, L, et al. *A Sharper View of the X-Ray Spectrum of MCG–6-30-15 with XRISM, XMM-Newton, and NuSTAR*. *ApJ* **2025**, *955*, 2, id200.
122. Gates, D. E. A., et al. *Morphology of relativistically broadened line emission from axisymmetric equatorial accretion disks*. *PRD* **2025**, *111*, 12.
123. Lowell, B., Jacquemin-Ide, J., Liska, M., et al. *PRD*, **2025**, *112*, 12, 123023.
124. Nekrasov, A. D., et al. *Relativistic reflection within an extended hot plasma geometry*. *A&A* **2025**, *704*, id. A129.
125. Palumbo, D. C. M. *Supermassive Black Hole Spin Constraints from Polarimetry in an Equatorial Disk Model*. *ApJL* **2025**, *978*, 1, id. L4.
126. Rosa, V., Foschini, L., & Ciroi, S. *Accretion and ejection at work in the Narrow Line Seyfert 1 galaxy 1H 0323+342*. *A&A* **2025**, *698*, A160.
127. Ricarte, A., et al. *Multimessenger Probes of Supermassive Black Hole Spin Evolution ApJ* **2025**, *980*, 1.
128. Walton, D. J., et al. *The broad-band view of the bare Seyfert PG 1426+015: relativistic reflection, the soft excess, and the importance of oxygen*. *MNRAS* **2025**, *543*, 3.
129. Cho, H., Prather, B. S., Narayan, R., et al. 2026, arXiv:2602.15560.
130. Madathil-Pottayil, A., et al. *Constraining black hole spin in PG 1535+547 amidst complex multi-layered absorption*. *MNRAS* Advanced Access **2026**.
131. Cruise, M., et al. *The NewAthena mission concept in the context of the next decade of X-ray astronomy*. **2024**. *Nature*, 9, pp. 36-44.
132. Lagard, M., et al. *The NewAthena X-ray optics*. **2025**. *SPIE Proceedings*, 13626.
133. Krumrey, M., et al. *Characterization of silicon pore optics for the NewAthena X-ray observatory*. **2024**. *Journal of Synchrotron Radiation*, 1600-5775.
134. Peille, P., et al. *The X-ray Integral Field Unit at the end of the Athena reformulation phase*. **2025**. *Experimental Astronomy*, **59**, 18.
135. Nandra, K., et al. *The Hot and Energetic universe: A White Paper presenting the science theme motivating the Athena+ mission*. **2013**. *White Paper*, arXiv: 1306.2307.